Review

Recent Developments in Electrode Materials for Oxygen Reduction Reaction

Rasu Ramachandran[1], Shen-Ming Chen[2,*], George peter Gnana kumar[3]

[1]The Madura College, Department of Chemistry, Vidya Nagar, Madurai – 625 011, Tamil Nadu, India.
[2]Electroanalysis and Bioelectrochemistry Lab, Department of Chemical Engineering and Biotechnology, National Taipei University of Technology, No.1, Section 3, Chung-Hsiao East Road, Taipei 106.Taiwan (ROC).
[3]Department of Physical Chemistry, School of Chemistry, Madurai Kamaraj University, Madurai-625 021,Tamil Nadu, India.
[*]E-mail: smchen78@ms15.hinet.net

Oxygen reduction reaction (ORR) has primary role in energy devices including green energy, light weight and low-cost alternative electrode materials. Recently, number of efforts was made to synthesis highly active electrode catalyst for energy harvesting and energy demands. The electrode catalysts have attracted much attention due to their physical and chemical properties. In this review, we mainly focused on different preparation methods developed for the production of different kinds of electrode materials, which could apply for ORR in fuel cell applications. The electrode materials such as nanoparticles, bimetallic, metal oxides, conducting polymers and nanocomposites have been reviewed in this article. Further developments in the fuel cell process will improve the pioneering electrode catalysis to contribute our future renewable some of energy storage devices.

1. INTRODUCTION

Oxygen reduction, fuel cells have generated considerable attention because of their potential alternative energy to serve as a low-cost, novel and eco-friendly source of electrical energy [1,2,3]. After the development of fuel cells have attracted and advanced electrode catalysis with their higher power density value of 2293 ± 50 mW m^{-2} in the recent reported literature [4]. A standard fuel cell consisting of a graphene-supported Pd and Pt catalyst used as a counter electrode [5]. Similarly,

bimetallic catalyst, in particularly graphene-supported Pd-Ru catalyst has been recognized as the most promising electrode materials for fuel cell applications. The active catalyst of 40 % Pd-5 % Ru/GNS electrodes catalytic activity ~2.6 times and the poisoning tolerance ~1.7 times greater than that of 40 % Pd/GNS modified electrode [6]. The different morphological studies, such as vertically aligned nanotube [7], bundle [8] and cylindrical [9] have been greatly interested, due to their unique mechanical properties and potential applications in a wide range of electrochemical applications. The most commonly used, modified electrode materials of GC with undoped and nitrogen doped multi-walled carbon nanotube showed a great promise a high electro catalytic activity for oxygen reduction in alkaline medium [10]. Recent developments of different electrode materials were used in various fields of energy storage devices [11,12,13] and electrochemical sensor [14,15,16] applications. Free-standing nitrogen-doped carbon nanotube/carbon nanofiber (NCNT/CNFs) fuel cells are typically coated uniformly, since the composite offer an excellent combination between electrical conductivity and good transparency [17]. One of the graphene-doped carbon nanotube showed a remarkable electrocatalytic activity towards oxygen reduction reaction than unmodified mesoporous xerol carbon electrode [18]. The novel carbon nanotube (CNT) supported stainless steel mesh (SSM) catalyst was a representative electrode materials, which can be used as a biocathode electrode material in the microbial fuel cell analysis. The biocathode of CNT-SSM catalyst achieved higher power density value of 147 mW m^{-2}, which was 49 times higher than that of bare SSM (3 mW m^{-2}) electrode [19]. Bimetallic (Pt-Co) nanoparticles were deposited on reduced graphene nanoplates (GNPs) based on gas diffusion layer (Carbon paper) (GDL) electrode (Pt-Co/GNP/GDL) by galvanostatic method. The mass activity of Pt-Co/GNP/GDL electrode founded to be high as 728.25 mA mg$_{pt-1}$ [20]. Alternatively, a simple, efficient and scalable approach of Vulcan XC-72 carbon-supported Pt nanoparticles has been synthesized by in situ hydrolysis and subsequent reduction method. The synthesized carbon-supported Pt NPs reported excellent catalytic activity, higher utilization efficiency and the high polarization performance [21]. A facile wet-chemical approach has been proposed to synthesis graphene nanosheet/three-dimensional Pt-on-Pd bimetallic nanodendrite (TP-BNGNG) hybrids using a 2D graphene nanosheet. In this study of TP-BNGN catalyst obtained much higher electrochemical performance than the conventional E-TEK Pt/C electrode [22]. Among the various electrode materials, Pt impregnated graphene nanofiber (GNF)-poly(3,4-ethylenedioxy thiophene) (PEDOT) composite was used as a promising catalyst, which would improve the electrocatalytic activity and its exhibit power density value of 537 mW cm^{-2} at loading current density 1120 mA cm^{-2} [23]. Yan *et al* [24] explored a typical platinum supported tungsten oxide with carbonized resin (Pt/C-WO$_3$) composite, which could apply fuel cell studies and the obtained kinetic mass current density value of 174.6 mA mg$_{pt}$$^{-1}$.

In this article, we present a systematic study of various electrode materials (Carbon, CNT, graphene, nanoparticle, metal oxides, bimetallic, conducting polymers and composites), electrode parameters, different analytical (SEM and AFM) and electro analytical (CV, RDE, EIS and Tafel) techniques has been explored for ORR. And also we highlighted various methods for the preparation/fabrication of potential electrode catalysts for the improvement of fuel cell performances.

2. ELECTRODE MATERIALS FOR ORR

2.1. Carbon electrode

A novel synthesis of platinum supported fish bone carbon nanofiber (CNF) for the study of the oxygen reduction reaction. The optimized catalytic activity of electrochemical surface area (ECSA) values exhibited at <20 m^2 g_{pt}^{-1} [25]. A facile electrodeposition route for the preparation of porous nitorgne-doped carbon nanofiber electrode has been focused on fuel cell application [26]. Lignin-derived electro spin carbon nanofibers (ECNFs) mate electrode deposited with Ag nanoparticle has been actively investigated for use in oxygen reduction in alkaline media fuel cell. The electrocatalytic activities have been optimized by cyclic voltammetry (CV) and rotating disc/rotating ring disc electrode (RDE/RRDE) method [27]. A novel nano scale metal-organic frameworks (MOFs) synthesized by the pyrolysis method showed superior electrocatalytic activity and good stability towards oxygen reduction in the alkaline medium.
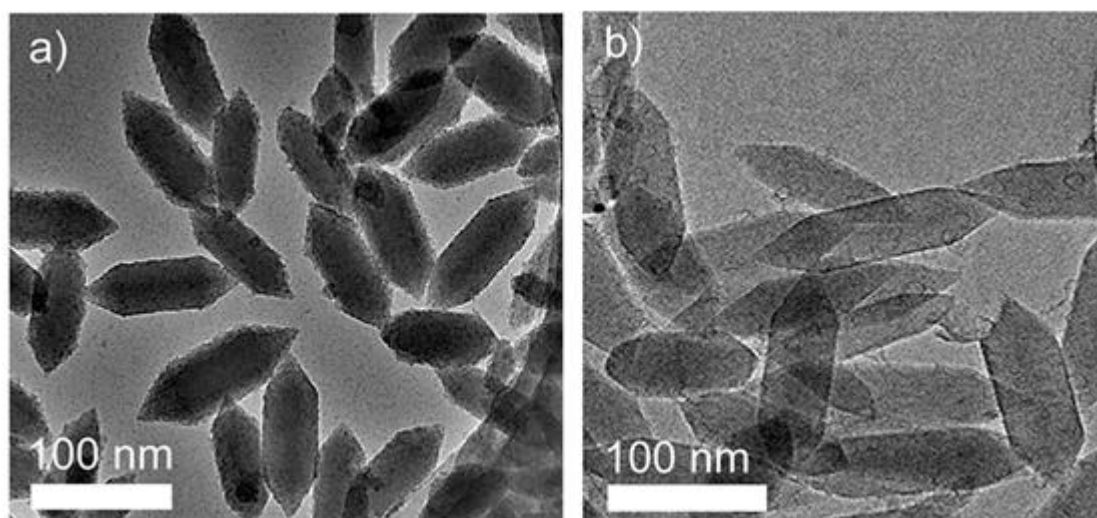

Figure 1. Shows (a and b) TEM images of nanoscale MIL-88B-NH$_3$ and CNPs. ("Reprinted with permission from (*ACS Nano* 8 (2014) 12660-12668). Copyright (2014) American Chemical Society").

The nano scale spindle-like MIL-88B-NH$_3$ NPs images are revealed that the uniform diameter (~50 nm) and length (~140 nm) (Fig.1) [28].Chemical activated nitrogen-doped carbon nanofiber (ANCNFs) was formed during through modified oxidative template assembly rout method and it was used as microbial fuel cell (MFC) catalyst exhibited a high power value of 1377 ± 46 mW m^{-2} [29]. Platinum and gold nanoparticles have been electrodeposited on innovative platelet carbon nanofiber composite offer a very sensitive electrocatalytic performance of direct methanol fuel cell application [30]. Tubular carbon nanofiber based electrode as an emerged another important class of material covering a broad range of polymer electrolyte membrane fuel cell studies [31]. A novel polypyrrole/Co-tetraphenyl porphyrin modified with carbon fibre paper (PPy/Co-TPP-CFP) electrode display fascinating fuel cell electrocatalytic properties of ORR [32].

2.2. Carbon nanotube

Electrocatalytic reduction of oxygen was investigated by using a modified carbon nanotube (CNT) and manganese oxide (MnO_2/CNT) composite. The maximum reported power density value of 210 mW m^{-2}, in these results are clearly indicating that CNT has an ideal catalyst support for modification of MnO_2. It can be also used as an alternative to Pt/C electrode for ORR [33]. The electrochemical behavior of ORR was studied at functionalized multi-walled carbon nanotube decorated with platinum nanoparticles (Pt/f-MWNTs) and platinum-cobalt alloy (Pt_3Co/f-MWNT) nanoparticle. The alloy modified electrode's obtained highest performs with a maximum power density value of 798 mW m^{-2} at 60° C [34]. The as-prepared low-cost and efficient phosphorous doped carbon nanotube and Pt (Pt/P-CNTs) electrode displayed significant enhancement electrocatalytic activity and long-durable stability of the strong interaction between Pt and P-CNTs.
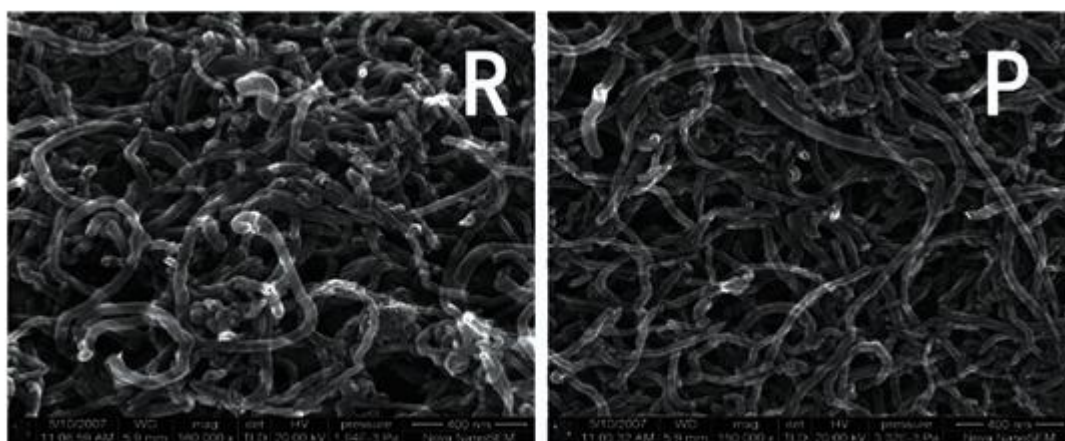

Figure 2. SEM images of *r*MCNTs (R) and *p*MCNTs (P). ("Reprinted with permission from (*J. Phys. Chem. C* 112 (2008) 2671-2677). Copyright (2008) American Chemical Society").

In Fig.2. Shows that the impurities of the metal nanoparticles were clearly appeared after the fabrication of MWCNT (Raw (rMWCNT) and purified (pMWCNT)) by the spontaneous formation method and exhibited higher electrocatalytic activity in ORR [35]. Gharibi *et al* [36] demonstrated the superior electrocatalytic role of the oxygen reduction reaction of nafion loaded platinum supported multi-walled carbon nanotube (Pt-MWCNT-nafion) composite. The comparison of nafion based composite and unmodified Pt/MWCNT electrode, Pt-MWCNT-nafion composite exhibit better performance in the ORR. The sputter coating method is widely used for preparing a non-precious nickel on to carbon nanotube on the carbon paper electrode. The optimized fabricated non-precious based composite reported promising electrocatalytic activity at the 850º C under ammonia environmental conditions [37]. Oxygen reduction reaction has been based on the other alternative conductive electrocatalytic activity, such as an ammonia-functionalized MWCNT supported iron phthalocynine (FePc) (*a*-MWCNT/FePc) composite for microbial fuel cell applications [38]. Yin et al [39] have described a polyaniline-cobalt-carbon nanotube (PANI-Co-CNT) nanocomposite modified

electrode based on electrocatalytic reaction, which they used to reduced oxygen. The number of electron ($4e^-$) studies has been optimized by rotating disc electrode (RDE) method.

2.3. Graphene electrode

The chemical exfoliation and functionalized of graphene have been synthesized for electrocatalytic fuel cell applications. The electrocatalytic performance of functionalized graphene (FG) found more than 45 % catalytic activity than commercialized carbon. The reported fuel cell power density values were found to be at different modified electrodes like Pt/C, Pt/G and Pt/FG and the exhibited values of 314, 426 and 455 mW cm^{-2} respectively [40]. A novel core-shell cyanamide cobalt complex embedded with a two-dimensional graphene sheet (g-C$_3$N$_4$@CoO/graphene sheet) composite for fuel (Oxygen reduction) cell studies. The observed graphene based composite displayed a four-electron transfer reaction and the obtained kinetic current density (J_k) value of 16.78 mA cm^{-2} [41]. Yan *et al* [42] used a nitrogen doped hallow mesoporous graphene sphere electrode for metal free electrocatalytic reactions and it can be applied in both anode and cathode of the fuel cell. Reduced graphene sheet (RGSs) has been synthesized by the chemical reduction method for the electrocatalytic study in 4-electron oxygen reduction reaction occurs at low over potential by using in neutral medium [43]. Similarly, a facile synthesis of nitrogen doped graphene (N-graphene) film by chemical vapor deposition (CVD) method. The film showed super performance in the study of oxygen reduction in alkaline medium fuel cell application. The catalytic current effect of N-graphene was found 3 times higher than that of Pt/C electrode [44]. Kataev *et al* [45] used lithium-based graphene electrode for oxygen reduction and exhibited sustainable energy storage device application. The top view SEM images of multi-layered graphene (MLG) and carbon nano-well (CNW) as shown in Fig.3 (a&b).
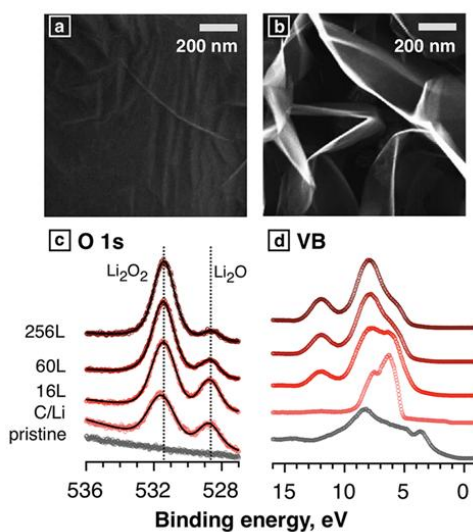

Figure 3. Top-view SEM images of the MLG (a) and CNW (b) samples. (c, d) O 1s and valence band photoemission spectra of pristine CNWs, lithiated CNWs, and the same sample during oxygen exposure. ("Reprinted with permission from (*ACS Nano* 9 (2015) 320-326). Copyright (2015) American Chemical Society").

The valence bond (O 1s) of pristine CNW was studied by using a photoemission spectroscopy as shown in Fig.3(c&d).

2.4. Metal oxides

Extensive studies have shown that the active cathode catalyst for PEFCs by used cost-effective electrode materials such as TiO_x, ZrO_x and TaO_x. Dip-coating method is one of the very simplest techniques for the preparation of these metal oxides and the titanium substrates were annealed at 400° C and 500° C. The annealed oxide electrode ($TiO_{0.7}$ $Zr_{0.3}O_x$/Ti) gives highest ORR [46]. The as-prepared and galvanostatic displacement methods for the fabrication of novel Pt-supported tungsten oxide electrode (Fig.4(A&B)).
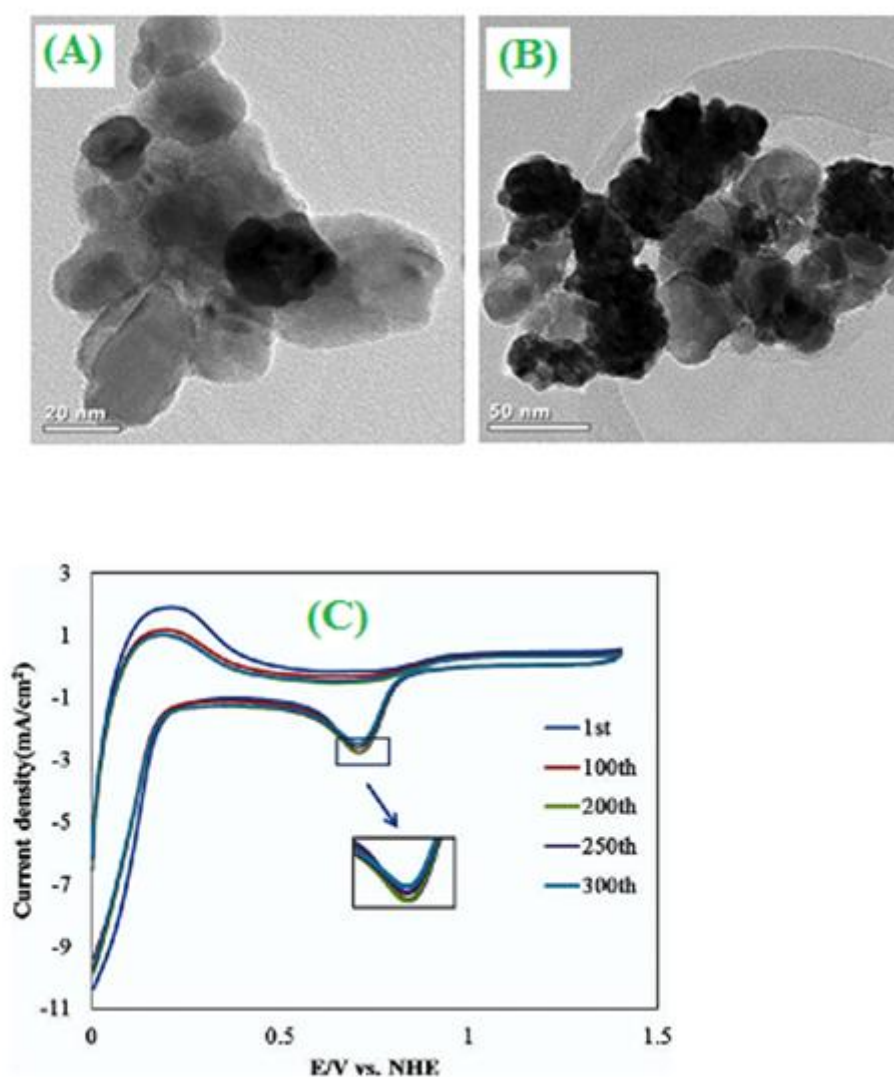

Figure 4. TEM (A) low (B) high images of Pt/WO_3 after cycling between 0 and 1.4 V 300 times. (C) Cyclic voltammograms of Pt/WO_3 in O_2 saturated 0.1 M $HClO_4$ between 0 and 1.4 V for 300 cycles; scan rate is 10 mV s^{-1}. ("Reprinted with permission from (*ACS Catal.* 2 (2012) 456-463). Copyright (2012) American Chemical Society").

The significant electrochemical performance in terms of electrocatalytic activity, which was Pt electrode surface area in ORR (Fig.4.C) [47].Chang and co-workers [48] showed that iridium oxide coated on the carbon electrode which can be used as a cathode material for ORR. The iridium based composite has been characterized by the cyclic voltammetry method, the onset potential was about 0.6 *vs* Ag/AgCl. The reported electrocatalytic power density value of 20 mW cm^{-2} and the achieved current density of 68.5 mA cm^{-2}. Perovskite $PrBa_x Co_2O_{5+\delta}$ (PB_x CO, x = 0.90-1.0) oxide electrodes have been shown to exhibit the intermediate solid oxide fuel cell (IT-SOFCs). PB_xCo cathode demonstrated that high electrochemical performance optimized by super low polarization resistance (R_p). A $Ce_{0.9}Gd_{0.9}O_{1.95}$ (CGO) electrolyte fuel cell with $PrBa_{0.94}Co_2O_{5+\delta}$ cathode obtained the attractive power density value of ~ 1.0 W cm^{-2} at 700° C [49]. Carbon supported cobalt-iron (II, III) oxides (Co-Fe_3O_4)/C hybrid nanoparticle exhibits relatively better catalysis of oxygen reduction in alkaline medium and the cathode can be used anion exchange membrane fuel cell (AEMFC). From the hydrodynamic voltametric studies, Co-Fe_3O_4/C gives four-electron (3.99) transfer involved in an electrochemical process. The ORR catalyst of Co-Fe_3O_4/C gives maximum performance of electrocatalytic activity with an applied open circuit potential (OCP) of 0.85 V *vs* RHE [50]. An *et al* [51] have used SSC (70 wt % $SrSc_{0.2}Co_{0.8}O_{3-\delta}$) − SDC (30 wt % $Sm_{0.2}Ce_{0.8}O_{1.9}$) composite for the evaluation of the intermediate-temperature solid-oxide fuel cell application. The composite showed highest electrocatalytic activity at 950° C and the delivered power density value of 760 mW cm^{-2} at 600° C.

2.5. Nanoparticle

Spray dying and hydrogen reduction method was prepared for a platinum nanowire network with silica based nanoparticle (Pt_{net}/SiO2) spacers for ORR. The TEM images of Pt_{net}/SiO$_2$ and Pt_{net}/C were observed the average diameter of 4.5 nm for Pt_{net}/SiO2 and 5.2 nm for Pt/C. The nanowire network electrode exhibited high electrochemical surface area (31.3 m^2 g$_{-pt}^{-1}$) and mass activity value of 110.5 A g$_{-pt}^{-1}$ at 0.85 V$_{RHE}$ [52]. Oezaslan *et al* [53] made a significant contribution in that of dealloyed Pt-Co$_3$ and PtCu$_3$ nanoparticle electrocatalytic reduction of oxygen. The nanoparticles were annealed at different temperatures such as 650°C, 800°C and 900°C for 7 hours. The maximum annealed (800°C & 900°C) sample (Pt-Cu alloy) showed most favourable mass activity and specific electrocatalytic (ORR) activity. A highly efficient and non-polluting energy conversion of nano sized Pt/IrO$_2$ electrocatalyst has been synthesized by the ultrasonic polyol method. The major application of iridium based electrocatalyst investigated for oxygen reduction and the reduction reaction in unitized regenerative fuel cell (URFs) to operate energy storage devices in conjugation with renewable power sources [54]. An outstanding electrocatalytic reduction of oxygen by barium carbonate (BaCO$_3$) nanoparticle in solid oxide fuel cell (SOFCs). The main objective of electrochemical impedance spectroscopy (EIS) analysis can greatly reduced in the interfacial polarization resistance of SOFC cathode materials includes $La_{0.8}Sr_{0.2}FeO_{3-\delta}$ (LSF), $La_{0.6}Sr_{0.4}Co_{0.2}Fe_{0.8}O_{3-\delta}$ (LSCF) and $La_{0.8}Sr_{0.2}MnO_{3-\delta}$ (LSM) [55]. Moreover, the other type of BaCO$_3$ nanoparticle, which is used to reduce oxygen on the $La_{0.8}Sr_{0.2}FeO_{3-\delta}$ (LSF) cathode for SOFCs based on ytrria stabilized zirconia (YSZ) electrolytes. The

interfacial polarization resistance value (2.96 to 0.84 Ω cm^2) was greatly reduced by using $BaCO_3$ nanoparticle and also the particle showed very good stability occur at 700°C under thermal conditions for 300 h [56]. Cheng *et al* [57] showed the in situ growth method of modified multi-walled carbon nanotube (*m*-MWCNT/Ag) nanoparticle composite electrode to exhibit electrocatalytic reduction properties towards the oxygen in alkaline medium.

2.6. Bimetallic

A thin film nanostructured (Fig.5.(A&B)) electrochemical de-alloying of ADP-Pt_2Ni_8 bimetallic catalyst for the reduction of oxygen and the remarkable electrocatalytic activity, which was 10-fold higher than that of commercial carbon supported Pt electrode (Fig.5.C) [58]. A carbon supported Pt_xFe alloy, which can be conventionally prepared by the glycerol-stabilized $NaBH_4$ reduction method for superior oxygen reduction for MFC. The maximum power density of Pt3-Fe/C (1680 ± 15 mW m^{-2}) higher than that of conventional Pt/C (1422 ± 18 mW m^{-2}) electrode respectively [59]. Silver-Cobalt (Ag-Co) is another typical bimetallic particle dispersed on a carbon powder (Ag-Co/C) which was prepared by Lima and their co-workers [60]. The number of electron transfer pathway which was analyzed by rotating disc electrode (RDE). The 4e$^-$ transfer pathway was exhibited on Ag on the Co_3O_4 site, besides 2e$^-$ transfer pathway has been reported on carbon and on the Co_2O_3 site etc.
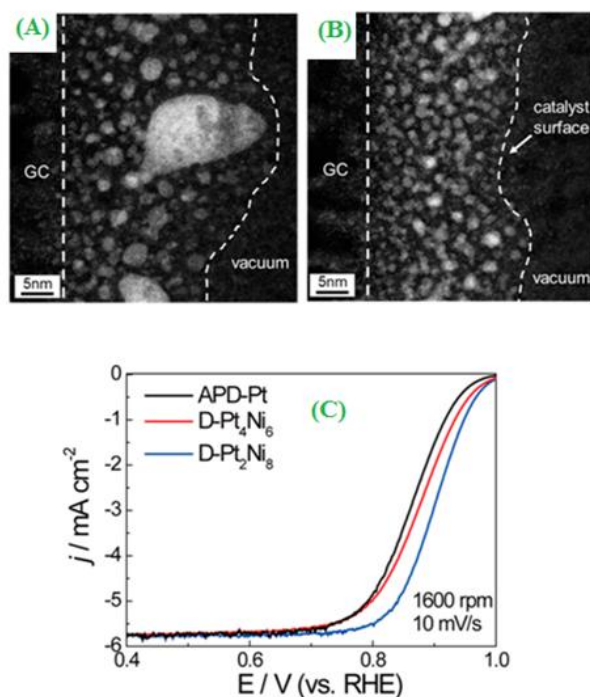

Figure 5. Cross-sectional HAADF-STEM images of Pt_2Ni_8 (as-prepared) (A) and D-Pt_2Ni_8 (de-alloyed) (B) on glassy carbon substrates. (C) Linear-sweep voltammograms for the ORR of D-Pt_4Ni_6, D-Pt_2Ni_8 and APD-Pt. ("Reprinted with permission from (*ACS Catal.* 5 (2015) 2209-2212). Copyright (2015) American Chemical Society").

The different ratios, carbon supported Pd and Pd_x Co alloy have been synthesized by the impregnation method at room temperature without heat treatment ethylene glycolic reduction conditions. Pd_xCo/C electro catalysis are widely used electrode material for the oxidation of methanol and also it can apply tolerant ORR catalyst in direct methanol fuel cell (DMFC) [61]. Salvo thermal method offers the opportunity has been prepared a monodispersed Au-Pd bimetallic alloy nanoparticle uniformly modified with reduced graphene oxide (RGO) and to disperse the enhanced electrocatalytic activity, better stability and good methanol tolerance towards ORR in alkaline conditions [62]. Carbon supported Pt/C and Pt-Pd/C nanoparticles have been synthesized by chemical reduction ($NaBH_4$) method. The Pt-Pd/C electrode showed higher electrocatalytic activity towards ORR in polymer electrolyte membrane fuel cell (PEMFCs) and the enhanced electro activity due to attributed a weakening of the O-O bond on Pd modified Pt nanoparticles [63].

2.7. Polymer electrolyte fuel cell

Nitrogen doped Australia's brown coal has been used as oxygen reduction reaction (ORR). The doped brown coal was characterized by a BET surface area (10 to 671 m^2/g) and rotating ring disk electrode (RRDE) [64]. Andreaus *et al* [65] have evaluated the physico-chemical origin of polymer electrolyte fuel cell analysis. Electrochemical impedance spectroscopy a study has been optimized the varying parameters, such as membrane thickness, humidification conditions and ionic intensity. The thicker membrane was strongly reduced at anode side by applying high current density at a low water content level. On the other hand, the catalyst site becomes inactive in dried medium. The polymer electrolyte fuel cell was studied by using a magnetic field gradient for electrochemical oxygen reduction. The electrochemical cell has fabricated a permanent magnet placed on the behind of cathode (Pt-dispersed carbon paper) electrode. The magnetized cathode exhibited oxygen reduction current was higher than the non-magnetized cathode [66]. Electro catalysis is frequently used for oxygen reduction of carbon supported platinum-vanadium alloy in polymer electrolyte fuel cell (PEFC) application [67]. Zhou *et al* [68] used the carbon supported Co-salen complex (Co-salen/C) by using methanol tolerance for polymer electrolyte membrane ORR. The electrode fabrication of a flexible polyvinyl chloride-silver coated electrode and then further electropolymerized with poly(phenyline oxide) to enhance the electrocatalytic activity [69].

2.8. Composite

A bifunctional based electrocatalytic of Au-MnO_2/MWCNT and Au-ZnO/MWCNT have been synthesized by chemical reduction of chloroauric acid. The applied electrocatalysis (oxygen reduction), the obtained maximum power density value of about 45 mW cm^{-2} and 56 mW cm^{-2} for Au-MnO_2/MWCNT and Au-ZnO/MWCNT respectively [70]. Electrophoretic deposition (EPD) and chemical bath deposition (CBD) have been used to fabricate a layer-by-layer assembled transparent amorphous Co_3O_4 nanoparticle/graphene (Co_3O_4/GR) composite on indium tin oxide (ITO). The Co_3O_4/GR composite reported electrocatalytic oxygen evolution exhibit significant catalytic activity

(High Faradaic efficiency, 95 %) and the excellent stability [71]. Tiido *et al* [72] have recently reported that a nano-sized Pt catalyst deposited onto titanium dioxide functionalized graphene nanosheet (TiO$_2$-FGSs) composite can serve as an excellent electrocatalytic reduction of oxygen. The TEM images of TiO$_2$-FGS were clearly indicated a good dispersion of Pt nanoparticle and the measured average particle size around 11 ± 2 nm. The composite electrode's catalytic activity has been optimized by Tafel and rotating disc electrode (RDE) method. The as-prepared graphene-iron phthalocyanine (*g*-Fe Pc) composite was improved oxygen reduction reaction and it possesses prominent catalytic activity [73]. Notably, salvothermal method has resulted in the formation of iron(III)tetracumyl phenoxy phthalocyanamine micro (FePc(CP)$_4$) on graphene (FePc(CP)$_4$/Gr) composite to developed oxygen reduction reaction studies [74]. Bo *et al* [75] have reported a good quality of aggregated and porous nitrogen-doped graphene (NGR) metal free-electrode for ORR fuel cell application.
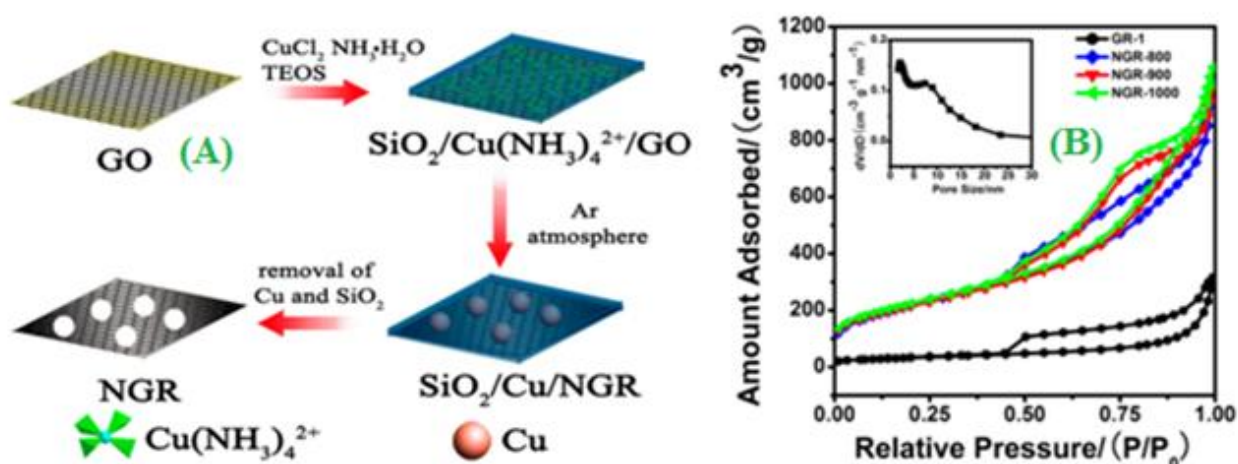

Figure 6. (A) Preparation Pathway of NGR (B) Nitrogen adsorption-desorption isotherms of NGR-800, NGR-900, NGR-1000, and GR-1. Inset: Pore size distribution of NGR-900. ("Reprinted with permission from (*ACS. Appl. Mater. Interfaces* 6 (2014) 3023-3030). Copyright (2014) American Chemical Society").

Fig. 6(A), the schematic illustration of the formation of NGR. The specific surface area also has been evaluated by N$_2$ adsorption-desorption isotherm method as shown in Fig.6(B).

3. EFFECT OF PARAMETERS

3.1. Effect of morphology

Loukrakpam *et al* [76] have used a heating treated carbon supported PtIrCo (PtIrCo/C) catalyst displayed excellent electrocatalytic activity in ORR. Transmission electron microscopy (TEM) of monodispersive nanoparticles, the average particle size of 2.5 nm (Fig.7). The double-layer capacitance studies of raw MWCNT and h-CNT electrodes. The calculated capacitance values were

obtained to be 916 μF cm^{-2} and 3254 μF cm^{-2}, from these values clearly indicate that annealed sample exhibits higher performance than raw electrode. The microspheres assembled KMn_8O_{16} nano rods have been synthesized by template-free hydrothermal method. The samples were annealed at various temperatures to optimize the highest performance of ORR and long-durability. The reported power density values were obtained 43.3 mW cm^{-2} for 25° C and 153.9 mW cm^{-2} for 70° C in direct methanol fuel cell (DMFCs) [77]. Iron based magnesium oxide (Fe/MgO) composite has produced on nitrogen doped carbon nanotube (N-CNT). Fe/MgO aging effect of carbon nanotube for 70 days aliquot sample, TEM morphology showed the average diameter is 50 nm and the resulted electrode materials organized by increasing the catalytic activity towards the electrochemical reduction of oxygen [78]. Yan *et al* [79] have prepared molybdenum oxide supported carbon material (C-MoO$_2$) by the ion-exchange method.
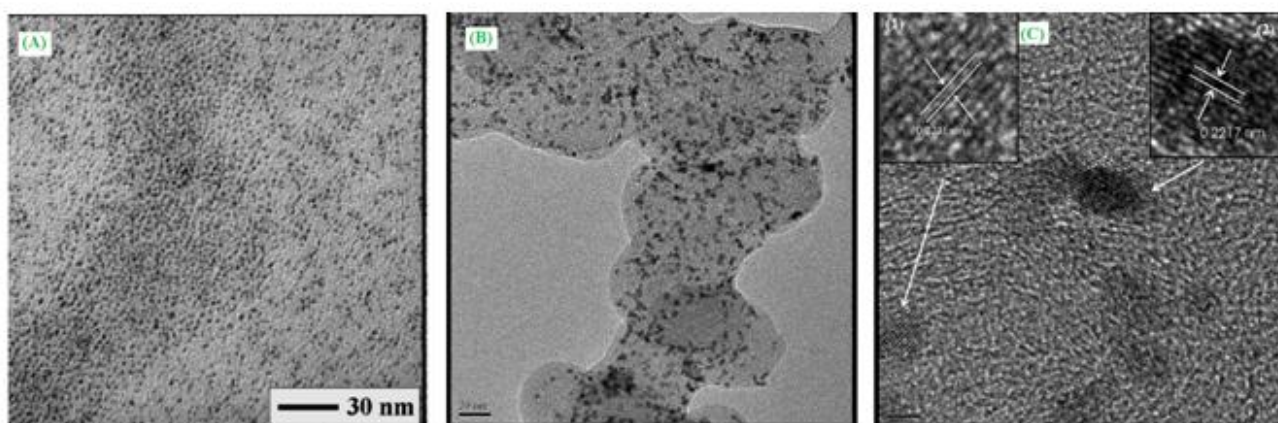

Figure 7. (A) TEM for a sample of as-synthesized $Pt_{25}Ir_{20}Co_{55}$ nanoparticles (2.2 ± 0.2 nm). (B) TEM (scale bar = 20 nm) and (C) HR-TEM (scale bar = 2 nm) for a sample of $Pt_{25}Ir_{20}Co_{55}$/C catalyst treated at 400° C. Inset: lattice fringes of (111) for the supported nanoparticles. ("Reprinted with permission from (*ACS Catal.* 1 (2011) 562-572). Copyright (2011) American Chemical Society").

The electrocatalytic study made with Pt nanoparticle on C-MoO$_2$ (Pt/C-MoO$_2$) composite gives high active and good electrocatalytic (ORR) properties. These results are clearly obtained from TEM images of Pt loading on C-MoO$_2$ at three different nanocrystal size levels like Pt/C-MoO$_2$ (0.50), Pt/C-MoO$_2$ (0.10) and Pt/C-MoO$_2$ (0.01). The activation of KOH with resulted in the formation of PNCN exhibit larger surface area and the comparable N$_2$ adsorption – desorption based PNCN Brunaure-Emmet Teller (BET) surface area value of 1392 m^2 g^{-1} and the carbonized sample of 183 m^2 g^{-1}. From the above observations, PNCN reported better catalytic activity and the power density value of 1159.34 mW m^{-2} [80]. Shi *et al* [81] have used a nitrogen and sulphur Co-doped mesoporous carbon material synthesized by the template method for ORR. The catalyst based electrode has been characterized by SEM, XRD, low temperature N$_2$ adsorption, X-ray photoelectron spectroscopy and rotating disc electrode (RDE).

3.2. Effect of surface roughness (AFM)

Zhu *et al* [82] have used $Co\text{-}S_2$ based thin film was prepared by magnetron sputtering method for the electrocatalytic reduction of oxygen. From the AFM analysis, the sputtered coated $Co\text{-}S_2$ film has a wrinkled surface around 80-100 nm and their estimated root-mean-square roughness value of 30 nm. Highly rough fractal-like type of Ru_xSe_y cluster catalyst has been synthesized by decorboxylation method and it can be used for polymer electrolyte membrane fuel cell. The optimized particle sizes range from 50 to 100 nm [83]. A simple chemical reduction of graphite oxide with the formation of reduced graphene sheets (RGSs) by applying with the sanction and it can further deposit on freshly cleaved mica as shown in the AFM analysis [84]. Strbac *et al* [85] used a spontaneous deposition of nanoisland rhodium on poly crystalline gold electrode for ORR. The size and surface topography of nanoisland rhodium has been optimized by AFM. Ensafi *et al* [86] have discussed for the wet chemical preparation of platinum supported reduced graphene oxide ($Pt^@SC_6H_4\text{-}rGO/GCE$) nanosheet catalyst in fuel cell applications. The surface behaviours of $3D\text{-}Pt^@rGO/GCE$ and $Pt^@SC_6H_4\text{-}rGO/GCE$ electrode catalysts have been investigated by AFM.

3.3. Effect of electrolyte

A highly orient of carbon-supported $Ni(OH)_2\text{-}MnO_x/C$ composite can be synthesized by using a reducing method in the presence of amorphous MnO_2/C and Ni^{2+} with $NaBH_4$. The most important consideration for use as alkaline media in the ORR studies. ORR study of $Ni(OH)_2\text{-}MnO_x/C$ composite, the accelerated agent electron transfer exhibits closes to four ie while for the $Ni(OH)_2\text{-}MnO_x/C$, MnO_2/C and MnO_x/C obviously exhibit from 3.88, 3.87 and 3.55 respectively [87]. The electroactive of $Mn_xCo_{3\text{-}x}O_4$ spinal thin films have been prepared by spray pyrolysis techniques [88]. The simple dispersion method provides a route for the preparation of a high surface area carbon supported iron phthalocyanine (FePc/C) composite electrode has been studied the polarization curve of ORR in acid medium. In the presence of methanol, FePc/C is insensitive and it becomes a more electrocatalytic performance than the Pt/C for ORR. FePc/C is proving to be very useful materials for fuel cell analysis, especially reduced the over potential and it acts as a good alternative electrode catalyst [89]. A well-dispersed peroveskite-type of $LaMnO_3$ supported nanoparticles were modified on pristine carbon black (CB) and graphitized carbon black (GCB) electrode by using sintering at different temperatures. The optimized mass ratio of 2:3 for carbon-$LaMnO_3$ exhibits highest electrocatalytic activity. In this high performance electrocatalytic activity was attributed due to the strong electrostatic interactions (C-O-M) between the metal oxides and carbon supported nanoparticles [90]. Extensive studies of nanoporous transition metal oxides of molybdenum, vanadium and tungsten oxynitrides have been synthesized by temperature-programmed ammonia reduction method for ORR catalyst in 0.1M KCl (pH = 5.6). The ORR mechanism has been analyzed by Koutecky-Levich equation and the exhibited electron transfer reaction was occurring at four [91].
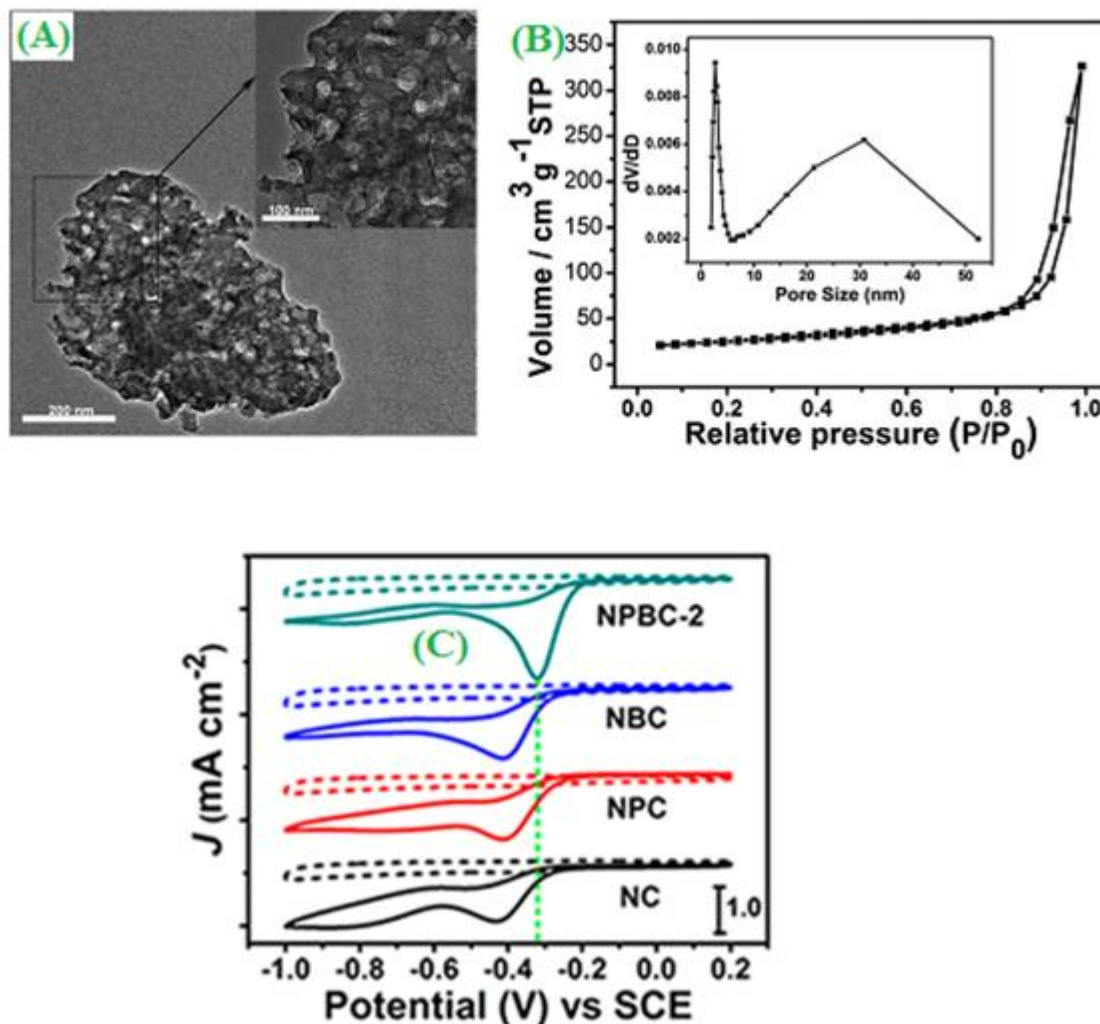
3.4. BET surface area

Figure 8. (A) Low-magnification and (inset) high-magnification TEM images of NPBC-2. (B) N_2 adsorption−desorption isotherms for NPBC-2 and (inset) the corresponding BJH pore-size distribution curve. (C) CV curves of NC, NPC, NBC, and NPBC-2 in (solid line) O_2-saturated or (dashed line) N_2-saturated 0.1 M KOH solutions with a scan rate of 50 mV·s^{-1}. ("Reprinted with permission from (*ACS. Appl. Mater. Interfaces* 6 (2014) 22297-22304). Copyright (2014) American Chemical Society").

The heteroatoms of nitrogen, boron co-doped carbon (NBC) and nitrogen-doped carbon (NC) electrodes have been synthesized by one-step pyrolysis method for their unique ORR studies. Fig.8.shows the nanoporous morphology of nitrogen-doped electrode catalysts have been studied N_2 adsorption-desorption, the obtained a typical hysteresis loop and the exhibited BET surface area of NBC of 89.5 m^2. g^{-1}, which was 2 times higher than that of NC (44.9 m^2. g^{-1}) electrode [92]. A globular shape of Nb-TiO$_2$ supported Pt (Nb-TiO$_2$/Pt) catalyst, which also become focused on intensive research owing to their unique application in ORR and the evaluated nitrogen sorption isotherm study of specific surface area (91 m^2 g^{-1}) was optimized by BET equation [93]. Matsubara *et al* [94] used a bamboo-shaped multi-walled carbon nanotube, which can be extensively studied the

activity of ORR and the measured BET surface area value of 157.71 m^2 g^{-1}. Platinum and palladium loaded nitrogen doped mesoporous carbon catalyst has widespread interest the catalytic properties for ORR. In this catalyst have great effort to improve the catalytic specific surface (BET) area assert a value of 900 m^2 g^{-1} [95]. The as-prepared platinum supported tungsten oxide (Pt/WO$_3$) nanosized catalyst was generally accepted to provide a good system to investigate the specific surface area (29.9 m^2 g^{-1}), which is reliable to the accepted theoretical value. In this optimized electrode catalyst to enhance the electrode catalytic activity towards the ORR [96]. Liu *et al* [97] showed that the nitrogen-doped hierarchical lamellar porous carbon was a synthesis from fish scales supported material for Pt nanoparticle. The novel hierarchical lamellar porous carbon exhibits the highest BET specific surface area value of 2730 m^2 g^{-1}.

4. TECHNIQUE FOR ORR

4.1. Cyclic voltammetry

Cyclic voltammetry is one of the mainly flexible electro analytical technique for the suggest the mechanism of electrochemical reactions. The most important two-dimensional and three-dimensional structure of Pt supported-cobalt nano wires (PtCoNWs) has been synthesized by the galvanic displacement method, the reported specific activity range 2053 – 2783 µA cm$_{pt}^{-2}$ (Fig.9) [98].
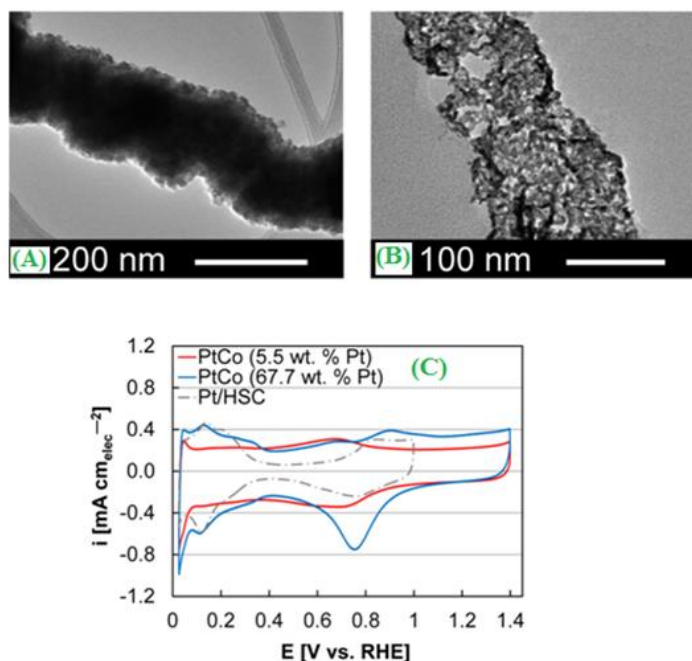

Figure 9. TEM images of PtCoNWs (21.1 wt % Pt): (A) assynthesized, (B) following electrochemical break-in (C) Cyclic voltammograms curves of PtCoNWs (5.5 and 67.7 wt % Pt with graphitized carbon nanofibers, 60 wt %, added to catalyst inks) and Pt/HSC. ("Reprinted with permission from (*ACS Catal.* 4 (2014) 2680-2686). Copyright (2014) American Chemical Society").

The development of a new carbon supported hype-type-d-electronic interactive nature of HT-Pt-TiO$_2$ composite catalyst comprising with Pt and Ti at three different atomic ratios (1:1, 2:1 and 3:1). The cyclic voltammetric studies, the optimized onset potential values for ORR on Pt/C, HT-Pt-TiO$_2$ (1:1)/C, HT-Pt-TiO$_2$ (2:1)/C and Pt-TiO$_2$ (3:1)/C catalysts are 0.89, 0.91, 0.99 and 0.98 V *vs* NHE respectively. The observed results are confirmed that HT-Pt-TiO$_2$ (2:1)/C and Pt-TiO$_2$ (3:1)/C showed higher catalytic activity than HT-Pt-TiO$_2$ (1:1)/C and Pt/C [99]. Use of a chemical vapor deposition (CVD) method for the synthesis of carbon coated tungsten oxide nano wires were directly grown on carbon paper (C-W$_{18}$O$_{49}$ NWs/carbon paper) and Pt nanoparticles were deposited on the (Pt/C-W$_{18}$O$_{49}$ NWs/carbon paper) composite. The specific surface area of Pt can be calculated by the following equation [100].

$$r_f \ (cm^2/cm^2{}_{pt}) = Q_M/0.21 \ mC/cm^2 \qquad\qquad\qquad\qquad Eq \ (1)$$
$$A_{pt} \ (m^2/g_{pt}) = r_f/[Pt] \qquad\qquad\qquad\qquad Eq \ (2)$$

Where Q_M is the mean of charge exchange during the hydrogen adsorption and desorption (mC/cm^2) and [Pt] is the platinum loading on the electrode surface area. Pt/C-W$_{18}$O$_{49}$ NWs/carbon paper composite electrode exhibits the mass surface area of 63.5 m^2/g$_{pt}$ higher than that of the commercial Pt/C electrode (40.6 m^2/g$_{pt}$). These results clearly indicate that, Pt/C-W$_{18}$O$_{49}$ NWs/carbon paper electrode more active than Pt/C electrode for ORR [101]. Chemical reduction (NaBH$_4$) allows the synthesis of carbon dispersed Pd$_5$Cu$_4$Pt nano catalyst for the importance of ORR in acidic conditions. Cyclic voltammetry study of carbon dispersed Pd$_5$Cu$_4$Pt are directly observed the proton adsorption-desorption peaks in the applied potential range of 0.05 – 0.30 V *vs* NHE in acid (0.5 M H$_2$SO$_4$) medium. By adding Pt nanoparticles, the peak values are shifted about 50 mV and the electro catalyst showed a maximum power density value of 330 mW cm^{-2} at 80° C [102]. A carbon black (CB) based platinum supported ceria (CeO$_x$) nanoparticle has been synthesized by the combined hot precipitation and impregnation method. The Pt-CeO$_x$/CB catalyst has been evaluated the surface chemical test, net chemical composition and electrochemical studies. The electrode stability (1000 cycles) test was optimized by the cyclic voltammetry method. The oxygen reduction reaction of Pt-CeO$_x$/CB exhibited higher catalytic activity than home-made Pt/CB catalyst [103]. Yuan *et al* [104] used amino functionalized multi-walled carbon nanotube (a-MWCNT) modified with iron phthalocyanine (FePC) (a-MWCNT/FePC) catalyst investigated the ORR. In this catalyst reported, a maximum power density of 601 mW m^{-2} and the hydrodynamic voltammetry optimized electron transfer was four (4e$^-$).

4.2. Polarization curves

New generation "shell" consisting of PtNi$_x$ alloy nanoparticles modified with carbon nitride (PtNi$_x$-CN) and a "core" of pyralyzed poly ketone nanotube (ST$_p$ = 500 to 900° C). The polarization and power curve "core-shell" matrix of PtNi$_x$-CN$_1$ 600/S700 and PtNi$_x$-CN$_1$ 900/S500 yielded higher fuel cell performance of ORR than PtNi$_x$-CN$_1$ 900/S700 and PtNi$_x$-CN$_1$ 600/S500 [105]. The catalytic activity of functionalized multi-walled carbon nanotube decorated with platinum nanoparticle (Pt/*f*-

MWCNT) and Pt-cobalt alloy nanoparticle (Pt$_3$Co/*f*-MWCNT) has been synthesized by conventional sodium boro hydride reduction and modified polyol reduction method. The polarization curve analysis of Pt$_3$Co/*f*-MWCNT electro catalysis has been optimized at three different annealed temperatures like 40, 50 and 60° C respectively. The electrochemical study of Pt$_3$Co/*f*-MWCNT yielded the highest performance with a maximum power density value of 798 mW cm^{-2} at 60° C for the cathode electrocatalysis for ORR in proton exchange membrane fuel cell (PEMFC) applications [34]. A dropping – calcinations method for the preparation of carbon-supported iridium oxide (IrO$_2$/C) catalyst as a cathode material by using ORR in polymer electrolyte fuel cell (PEFC) application. IrO$_2$/C catalyst has been characterized by cyclic voltammetry and polarization curve method. From the polaragram and power density curves, the applied open circuit voltage (OCV) was 0.80 V and the cell voltage of 0.2 V results the limiting current density of 34 mA cm^{-2} and the power density value of 6.8 mW cm^{-2} [106]. Zhang *et al* [107] reported palladium-iron (PdFe) based nanoleaves electrode catalyst for ORR by solution phase reduction rout. The polarization curve analysis of the electrode, which was used as the highly electrocatalytic active and a promising new class of cathode electrode for anion exchange membrane fuel cell application as shown in Fig.10. A novel catalyst of manganese-polypyrrole-carbon nanotube (Mn-PPY-CNT) composite has been synthesized by the salvo thermal method for the reduction of oxygen in microbial fuel cell (MFC) applications.

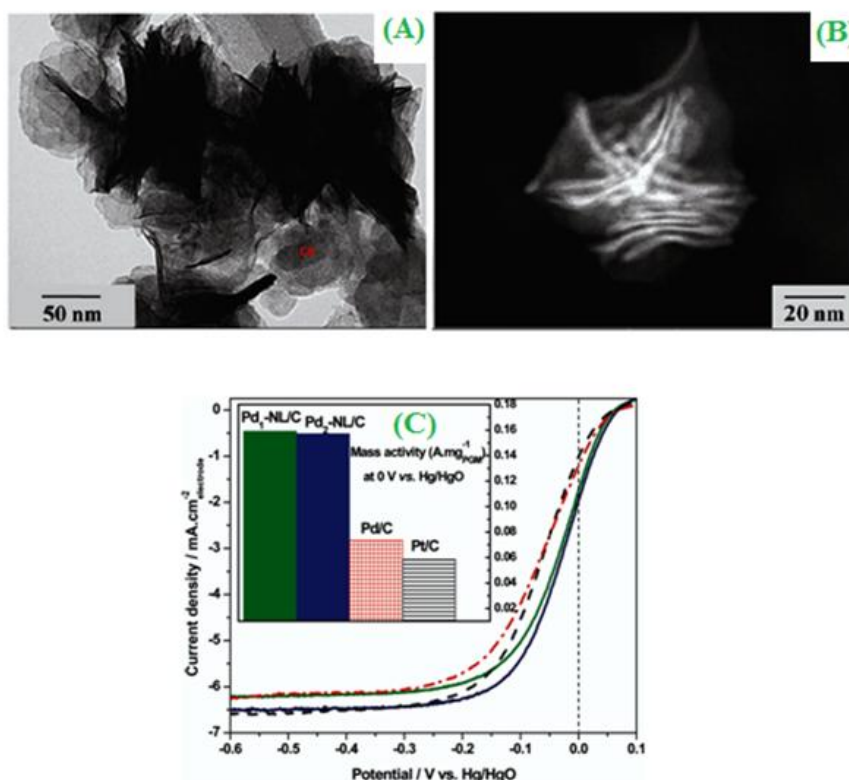**Figure 10.** Morphology of Pd$_1$-NL/C (Pd$_1$Fe$_1$-NL/C after acid treatment): (A) TEM image, (B) HAADF-STEM image (C) ORR polarization curves of commercial Pt/C, Pd/C (self-prepared by EG method), Pd$_1$-NL/C and Pd$_2$-NL/C in 0.1 M NaOH, O$_2$ bubbling (conditions: 10 mV s^{-1}, 2500 rpm, room temperature). ("Reprinted with permission from (*Chem. Mater.* 23 (2011) 1570-1577). Copyright (2011) American Chemical Society").

The manganese based (Mn-PPY-CNT) catalyst loading of 1 mg cm^{-2} has produced the power density value of 169 mW m^{-2}. When the catalyst loading increases (2 mg cm^{-2}), the power density values also increases (213 mW m^{-2}) [108]. A very interesting corrugated morphology of nitrogen doped carbon nanotube (NCNTs) has been synthesized by the chemical vapor deposition method for highly active ORR. NCNTs catalyst exhibits superior mechanical, thermal, inexpensive and highly stable for ORR [109]. Lou *et al* [110] used a carbon and pt supported core-shell structure alloy for ORR by microwave-assisted polyol and chemical dealloying method. Polarization curve has developed the electrocatalytic activities from the estimated half-wave potential values.

4.3. Rotating disc electrode (RDE)

The sputter coating method offers a mesoporous platinum-cobalt alloy catalyst with significant enhancement of ORR in PEMFC. By using RDE, a micro structural and compositional parameter of the kinetic current j_{kin} has been optimized by the following eq. (3).

$$j_{kin} = \frac{j_{dif \times j}}{j_{dif - j}} \qquad \text{Eq. (3)}$$

Where j_{dif} is the limited measured over the applied potential range between 500 mV and 100 mV *vs* NHE [111]. The inherently electrocatalysis of multi-walled carbon nanotube supported Pt-Pd (Pt-Pd/MWCNT) nanoparticles were prepared by chemical reduction (NaBH$_4$) method in PEMFCs. The catalyst was analyzed by using cyclic voltammetry (CV) and rotating disc electrode (RDE) method. From the linear scan voltammogram (RDE), plots of the limiting current against the square root of various rotation speed value by using Koutecky-Levich plot. The direct electrochemical reduction of oxygen follows a two-step 4e$^-$ reduction pathway of O$_2$ to H$_2$O [112]. A carbon-supported Co-salen complex (Co-salen/C) was pyralized at different temperatures (600, 700, 800, 900 and 1000° C) to form the other type of carbon-supported Co-N-S/C catalyst for the use of electrocatalytic (ORR) reactions. The annealed (700° C) catalyst (Co-N-S/C) gives strong electro catalytic activity and the estimate overall electron transfer number of about 3.6-3.9 towards the ORR by using RDE [113]. Millan *et al* [114] used a platinum-free carbon supported-conducting polymer based, cobalt (Carbon/polyaniline/cobalt, carbon/polypyrrole/cobalt and carbon/poly(3-methylthiophene)/cobalt) catalyst for the study of ORR. Zhang and co-workers [115] showed three different electrocatalysis (PdPt nanocage/C, Pd@Pt nanodendrites/C and Pt/C) for the evaluation of fuel cell application. Kinetic study of ORR and the electron transfer reaction have been optimized by RDE. The calculated electron transfer reaction which was 3.8 for Pd@Pt NDs/C, 3.8 for PdPt NCs/C and 3.9 for Pt/C respectively. By the preparation in a carbon supported Pt-Co alloy and polyoxometallates Cs$_{2.5}$H$_{0.5}$Pw$_{12}$O$_{40}$ composite as an electrocatalyst, which can be employed for the estimation of mass activity and high electrochemical performance [116].

4.4. Power density

Jung *et al* [117] have used a comparable four different Pt, Pd and carbon supported (Pd/C, Pt-Pd/C-H, Pt-Pd/C-N and Pt/C) electro catalysts prepared by conventional reduction and sequential

impregnation methods. The electrode materials have been discussed for the study of ORR and the observed power density values were measured to be the increasing the following orders such as Pd/C< Pt-Pd/C-H< Pt-Pd/C-N< Pt/C (255.1< 383.6< 480.5< 543.1). The method of electro catalyst was originally developed by Liu *et al* [118] and consists of renewable, low-cost and sustainable nitrogen, phosphorous dual-doped carbon catalyst for microbial fuel cells (MFCs). The dual-doped $(NH_4)_3PO_4$-carbon catalyst, delivered maximum power density value (2293 ± 50 mW m^{-2}) than the control reference study of Pt/C based catalyst (1680 ± 32 mW m^{-2}). Another important approach is the intermediate optimized temperatures (80-130° C) carbon supported PtCo catalyst (Pt_3Co_1/C) focused on a superior catalytic activity in PEMFCs and it exists good stability with respect to the conventional Pt/C catalyst. The electro-kinetic parameters of reaction order and activation energy have been determined by a steady-state of the galvanostatic polarization curve method. The observed negative activation energies of 40 kJ mol^{-1} and 18 kJ mol^{-1} were occurring at 0.9 V and 0.65 V respectively. The influencing of temperatures under high pressure (3 bar abs) operating conditions exhibited maximum power density of 934 mW cm^{-2} at 80° C and 990 mW cm^{-2} at 100° C [119]. A novel-hybrid carbon supported binuclear-cobalt-phthalocyanine (Bi-CoPc/C) was integrated with metal oxides (NiO and CoO) to form a macro cyclic complex for the enhancement of electrocatalytic (ORR) activities. The cyclic voltammetry study showed the nickel based catalytic (Bi-CoPc/C-NiO) reduction peak potential at -0.12 V and cobalt based catalytic (Bi-CoPc/C-CoO) reduction peak potential at -0.22 V respectively. Among these tested catalysts, Bi-CoPc/C integrated metal oxide showed potential electrode material to replace the cost Pt electrode catalyst [120]. Among the above discussed catalyst method, hydrothermal was one of the important methods for the preparation of biomass carbon supported silver-tungsten carbide nanohybrid (Ag-WC/C) catalyst for ORR in MFC under neutral (pH = Phosphate buffer) medium. Ag-WC/C catalyst has been characterized by the powder X-ray diffraction and transmission electron microscopic (Average particle size about 14 nm) methods [121]. A novel and efficient cost effective stainless steel mesh/cobalt hydroxide (SSM/Co_3O_4) electrode was synthesized by a simple ammonia-evaporation induced method for MFCs [122].

4.5. Performance of fuel cell

A cerium-zirconium oxide ($Ce_{0.8}Zr_{0.2}O_{0.2}$) (CZO) has been synthesized by co-precipitation method. The CZO metal oxide catalyst mixed with carbon-supported platinum (Pt/C) catalyst to form $Ce_{0.8}Zr_{0.2}O_{0.2}$-Pt/C. X-ray photoelectron spectroscopy (XPS) has been proved the oxidation states of (Ce^{3+} and Ce^{4+}) cerium oxide and to study the oxygen storage and release the mechanism. The fuel cell performance of $Ce_{0.8}Zr_{0.2}O_{0.2}$-Pt/C catalyst was optimized at different temperatures and the exhibited high performance (322 mW cm^{-2}) fuel cell observed at 55° C [123]. Highly active carbon-supported platinum modified cobalt (PtCo/C) catalyst was firstly formed during ethylene glycol (EG) reduction method and it can be used as an electro catalyst for PEMFC applications. The de-alloying and heat treatment PtCo/C catalyst was highly effective for improving the performance activity and the active component particles were uniformly dispersed a narrow distribution particle size around 2-4 nm [124]. A novel traditional polyol method was developed to form the nafion stabilized $Ir_{85}Se_{15}$/C catalyst for

ORR in PEMFC. The catalytic cell performance of Nafion- $Ir_{85}Se_{15}/C$ catalyst obtained the maximum power density value of 736 mW cm^{-2}, which it was 1.8 times higher than that of $Ir_{85}Se_{15}/C$ [125].

4.6. Tafel plot

Multi-walled carbon nanotube was immobilized with laccase on the disc electrode using 1-pyrenebutanoic acid succinimidyl ester.
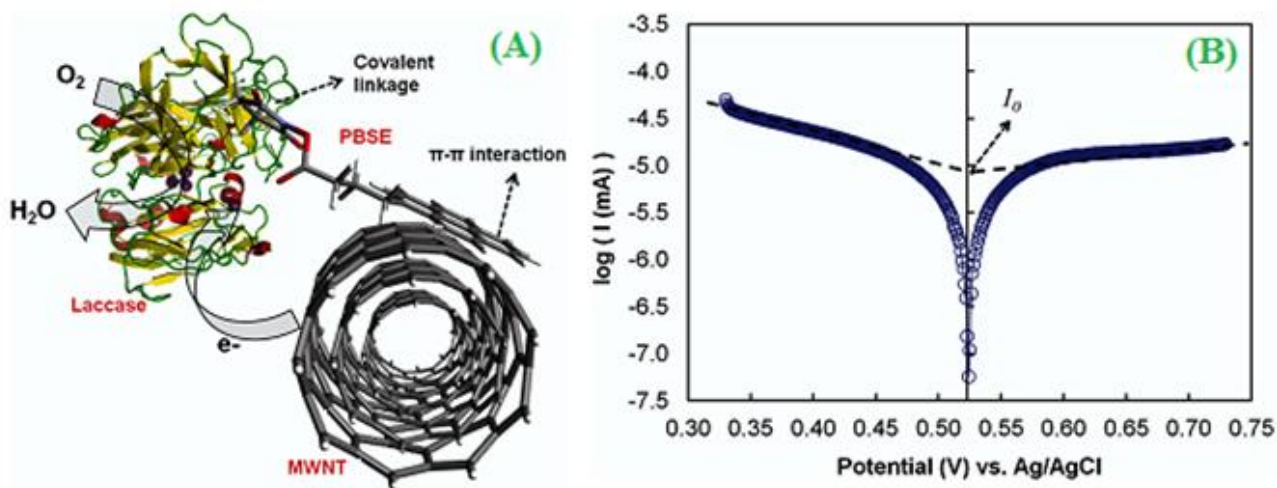

Figure 11. (A) Schematic of the bio-nanocomposite where laccase is tethered to MWNT using pyrenebutanoic acid succinimidyl ester (PBSE). (B) Linear sweep voltammograms showing Tafel regions at no rotation for the laccase-MWNT in phosphate buffer (pH 5.8). The applied potential range was from 0.33 to 0.73 V. ("Reprinted with permission from (*ACS Catal.* 2 (2012) 38-44). Copyright (2012) American Chemical Society").

The schematic representation of the bio-composite was explained that a covalent bonding of the protein and non-covalent functionalized MWCNT, π-π interactions (Fig. 11(A)). From the Tafel slope, the equilibrium exchange current density (I_0 = 3.3 x 10^{-5} A cm^{-2}) and electron transfer rate (k_{et} = 6.72 x 10^{-5} cm s^{-1}) have been estimated (Fig. 11(B)) [126]. Schmidt *et al* [127] suggested that carbon supported platinum (Pt/C) catalyst can be explored to be very promising electrode materials for ORR in different chloride anions. The smooth polycrystalline and single crystal Pt/C catalyst's fuel cell activities decreases in the following orders like ClO_4^- > HSO_4^- > Cl^-. This is due to clearly explain that the increasing adsorption bond strength of the anions. The high - surface area of Pt/Vulcan XC 72 has been optimized by the anion effect using thin-film rotating ring disc electrode (RRDE). Comparable measurements were carried out at low temperature (60° C), electrolyte with weak adsorbing (ClO_4^-), modestly strong adsorbing (HSO_4^-) and strongly adsorbing (Cl^-) by using different concentrations of electrolytes. Electrodeposited ultrafine carbon black supported TaO_x (TaO_x/CB) catalyst can serve as a electrocatalytic reduction of oxygen in PEFC. The catalyst has been characterized by SEM, STEM, XPS and electron energy-loss spectroscopic (EELS) methods. The catalyst powders were removed from the deposited electrode and subsequently it gives hydrogen treatment at varying temperatures

(523 and 1073 K) to enhance the fuel cell performance. The specific annealed (873 K for 2 Hrs) catalyst with nafion ionomer exhibits higher activity and the applied onset potential value of 0.95 V vs RHE at -2mA cm^{-2}. At the end of the 1000th cycle experiment, only 6 % samples were degraded, other than remaining 94 % sample was retained. Tafel slope of TaO$_x$/CB catalyst showed the slope of ~ 0.093 V dec^{-1} and the ORR catalyst have confirmed that one-electron transfer occurs in the rate determining step [128]. There has been an explosive study of nitrogen-containing carbon nanostructures (Fiber diameter, fiber type and N-content) were synthesized by the decomposition of acetonitrile at 900° C over silica and magnesia impregnated with Fe, Co and Ni. The nanostructures of CN$_x$ nanofiber have been examined the electrochemical properties such as activity, conductivity and selectivity if ORR reduced to water. Tafel study one of the useful analyses for the comparison of electrochemical studies and fuel cell performance. These slopes were plotted from the kinetic controlled current against rotation speed (1000 rpm) in O$_2$. From this type of analysis, less active samples exhibited higher slope [129]. Well defined copper-platinum (Cu-Pt) nanotubes were synthesized by the galvanostatic replacement reaction method. The SEM images are clearly shown that a well-defined Cu-Pt nanotubes, the approximate diameter 100 nm in diameter. The various ratios electro catalysis of Cu-Pt nanotubes was deduced the kinetic parameters obtained from the Tafel slope for ORR [130].

4.7. Electrochemical impedance spectroscopy (EIS)

The EIS is a time-dependent perturbation signal, applied frequency and sinusoidal voltage. The state of art of N$_d$BaCo$_2$O$_{5+\delta}$ cathode electrode catalysis, the electrochemical reduction of oxygen reaction used in intermediate-temperature solid oxide fuel cell (IT-SOFCs). In the development of Nyquist diagram showed at the three different changes with applied three different temperatures as well the applied potential such as at 500 and 550° C, at 600° C, at 650 and 700° C, which could be related the changes in the charge-transfer and oxygen diffusion processes including oxygen adsorption or desorption processes [131]. The conventional method is very useful technique for the preparation of Pd-Y$_2$O$_3$ stabilized ZrO$_2$ (YSZ) composite for IT-SOFCs. The cathode with 5 wt % Pd loading demonstrates the lowest polarization resistance value, while 0.5 wt % of Pd loaded sample, the R$_{CT}$ value exhibited highest polarization resistance value. This is due to display that, Pt-YSZ-2 cathode used as an optimized polarization resistance value and this catalyst exhibited good electrochemical performance studies [132]. The electro active platinum supported fish bone carbon nano fibres (Pt/CNF) have been explored extensively used for ORR. The different electrochemical performance was observed from the Nyquist plot. In this EIS analysis has been used four different catalysts like Pt/CNF 550, Pt/CNF 600, Pt/CNF 700 and Pt/Vulcan etc. On the basis of R$_{CT}$ observed values, Pt/CNF 700 catalyst reported highest fuel cell performance at low temperature (30° C) [25]. Shanmugam *et al* [133] have used a newly synthesized globular morphology of platinum supported titanium oxide (Pt/TiO$_2$) catalyst has been applied in ORR. The better electrocatalytic activity, which was estimated from the Nyquist plot (Fig.12). Table.1. Shows that, the comparative study of preparation methods,

different electrode catalysis, surface morphology, annealing temperature and the evaluation of various electrocatalytic performances of ORR in fuel cell applications.
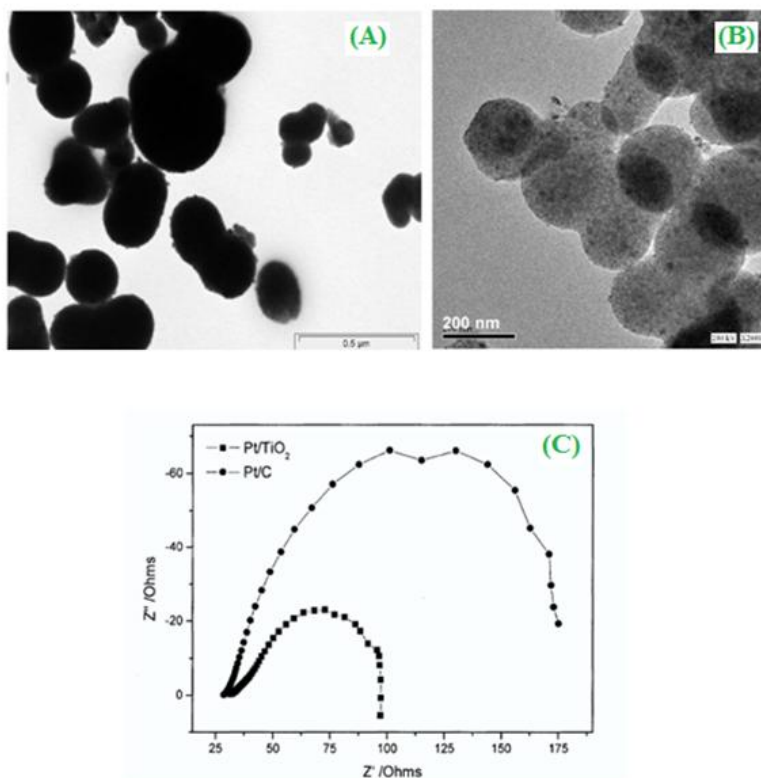

Figure 12. TEM images of (A) TiO_2 and (B) Pt/TiO2 (C) Nyquist plot for the electrodes (Pt/TiO_2 and Pt/C) in 0.5 M H_2SO_4 at open circuit potential. ("Reprinted with permission from (*J. Phys. Chem. C* 113 (2009) 18707-18712). Copyright (2009) American Chemical Society").

Table 1. Summary of different electrode catalyst, methods, size, conditions and power densities of oxygen reduction reaction

S.No	Catalyst	Method	Particle size (nm)	*T*/°C	Power density	Rf.
1	Carbonaized nanoparticle	Hydrothermal	50-140	60°C	22.7 mW cm^{-2}	[134]
2	Carbon supported Ir_xSe_y Chalcogenide	Micro-wave	1.53-2.39	-	500 mW cm^{-2}	[135]
3	Graphene wrapped	CVD				[136]
	MWCNT		60-70	-	661 mW cm^{-2}	
	Pt/GC-240		120-140	-	653 mW cm^{-2}	
	Pt/GC-500					
4	Carbon supported Pt NPs	Chemical reduction	3.5-4.8	-	451 mW cm^{-2}	[137]
5	Graphene nano fiber/PEDOT*	Electrochemical reduction	-	70°C	537 mW cm^{-2}	[23]

6	CNT supported aerogel carbon	Pyrolysis	20-50	60°C	10 mW cm^{-2}	[138]
7	Porous carbon paper	Functional	-	-	783 mW cm^{-2}	[139]
8	Co/Fe/N/CNT	Commercial functionalization	-	-	751 mW m^{-2}	[140]
9	Mn-PPY-CNT	Solvothermal	-	-	213 mW m^{-2}	[141]
10	CNTs-SSM	Chemical	-	-	147 mW m^{-2}	[142]

*PEDOT – Poly(3,4-ethylenedioxythiophene); *Mn-PPY-CNT – Manganese-polypyrrole-carbon nanotube; *CNTs-SSM – Carbon nanotubes-stainless steel mesh; *CVD – Chemical vapor deposition.

5. CONCLUSIONS

In this work, we have demonstrated the various electrode materials and fabrication methods to study ORR in fuel cell analysis. The discussed electrode catalyst explored excellent electrocatalytic properties towards ORR with supporting of their respective applied potential and the limiting current density values. These include fabrication of modified (Carbon, metal, metal oxides, conducting polymers and composites) electrodes and greatly enhanced the electrode catalytic activity of ORR in FCs. In most of the analytical and electro analytical (experimental) findings were in good agreement with the many of reported literature, which was the optimization of annealed temperature, morphological studies and long-duration of electrode stability of ORR.

References

1. B. Li, X. Zhou, W. Wang, B. Liu, B. Li, *J. Power Sources* 272 (2014) 320-327.
2. B.R. Camacho, J.H.M. Gonzaloz, R.G.G. Huerta, M.T. Velazquez, *Int. J. Hydrogen Energy* 39 (2014) 16731-16739.
3. M. Yaldagard, N. Seghatoleslami, M. Jahanshahi, *Appl. Surf. Sci.* 315 (2014) 222-234.
4. Q. Liu, Y. Zhou, S. Chen, Z. Wang, H. Hou, F. Zhao, *J. Power Sources* 273 (2015) 1189-1193.
5. M.H. Seo, S.M. Choi, H.J. Kim, W.B. Kim, *Electrochem. Commun.*, 13 (2011) 182-185.
6. R. Aswathi, R.N. Singh, *Carbon* 51 (2013) 282-289.
7. W.Y. Wong, W.R.W. Daud, A.B. Mohamad, A.A.H. Kadhum, K.S. Loh, E.H. Majlan, *Int. J. Hydrogen Energy* 38 (2013) 9421-9430.
8. H. Li, H. Liu, Z. Jong, W. Qu, D. Geng, X. Sun, H. Wang, *Int. J. Hydrogen Energy* 36 (2011) 2258-2265.
9. D.H. Raja, DD.P. Pandiyan, Energy Procedia 22 (2012) 67-77.
10. M. Vikkisk, I. Kruusenberg, V. Joost, E. Shulga, K. Tammeveski, *Electrochim. Acta* 87 (2013) 709-716.

11. R. Ramachandran, V. Mani, S.M. Chen, R. Saraswathi, B.S. Lou, *Int. J. Electrochem. Sci.* 8 (2013) 11680-11694

12. S.M. Chen, R. Ramachandran, V. Mani, R. Saraswathi, *Int. J. Electrochem. Sci.* 9 (2014) 4072-4085.

13. R. Ramachandran, S.M. Chen, G.P. Gnanakumar, P. Gajendran, N. Birunthadevi, M. Govindasami, *Int. J. Electrochem. Sci.* 10 (2015) 859-869.

14. R. Ramachandran, V. Mani, S.M. Chen, G. Gnanakumar, M. Govindasamy, *Int. J. Electrochem. Sci.* 10 (2014) 859-864.

15. K.J. Babu, A. Zahoor, K.S. Nahm, R. Ramachandran, M.A.J. Rajan, G. Gnanakumar, *J. Nanopart. Res.* 16 (2014) 2250-2259.

16. V. Mani, R. Devasenathipathy, S.M. Chen, K. Kohilarani, R. Ramachandran, *Int. J. Electrochem. Sci.* 10 (2015) 1199-1207.

17. Q. Guo, D. Zhao, S. Liu, S. Chen, M. Hanif, H. Hou, *Electrochim. Acta* 138 (2014) 318-324.

18. C. Arbizzani, S. Righi, F. Soavi, M. Mastragostino, *Int. J. Hydrogen Energy* 36 (2011) 5038-5046.

19. Y. Zhang, J. Sun, Y. Hu, S. Li, Q. Xu, *J. Power Sources* 239 (2013) 169-174.

20. M. Yaldagard, N. Seghatoleslami, M. Jahanshahi, *Appl. Surf. Sci.* 315 (2014) 222-234.

21. H.Y. Park, D.S. Yang, D. Bhattacharya, M.Y. Song, J.S. Yu, *Int. J. Hydrogen Energy* 39 (2014) 1688-1697.

22. S. Guo, S. Dong, E. Wang, *ACS Nano* 4 (2010) 547-555.

23. S.G. Peera, K.K. Tintula, A.K. Sahu, S. Shanmugam, P. Sridhar, S. Pichumani, *Electrochim. Acta* 108 (2013) 95-103.

24. Z. Yan, W. Wei, J. Xie, S. Meng, X. Lu, J. Zhu, *J. Power Sources* 222 (2013) 218-224.

25. D. Sebastian, M.J. Lazaro, I. Suelves, R. Moliner, V. Baglio, A. Stassi, A.S. Arico, *Int. J. Hydrogen Energy* 37 (2012) 6253-6260.

26. J. Yin, Y. Qiu, J. Yu, *J. Electroanal. Chem.* 702 (2013) 56-59.

27. C. Lai, P. Kolla, Y. Zhao, H. Fong, A.L. Smirnova, *Electrochim. Acta* 130 (2014) 431-438.

28. S. Zhao, H. Yin, L. Du, K. Zhao, L. Chang, G. Yin, H. Zhao, S. Liu, Z. Tang, *ACS Nano* 8 (2014) 12660-12668.

29. X.Yang, W. Zou, Y, Zu, Y. Zou, H. Jiang, J. Shen, *J. Power Sources* 266 (2014) 36-42.

30. L. Giorgi, E. Salernitano, T.D. Markris, S. Gagliardi, V. Contini, M.D. Francasco, *Int. J. Hydrogen Energy* 39 (2004) 21601-21612.

31. E. Wallnofer, M. Perchthaler, V. Hacker, G. Squardrito, *J. Power Sources* 188 (2009) 192-198.

32. W. Zhang, J. Chen, P. Wagner, G.F. Swiegers, G.G. Wallace, *Electrochem. Commun.*, 10 (2008) 519-522.

33. Y. Zhang, Y. Hu, L. Li, J. Sun, B. Hou, *J. Power Sources* 196 (2011) 9284-9289.

34. B.P. Vinayan, R.M. Jafri, R. Nagar, N. Rajalakshmi, K. Sethupathi, S. Ramprabhu, *Int. J. Hydrogen Energy* 37 (2012) 412-421.

35. Z.D. Wei, C. Yan, Y. Tan, L. Li, C.X. Sun, Z.G. Shao, P.K. Shen, H.W. Dong, *J. Phys. Chem. C* 112 (2008) 2671-2677.

36. H. Gharibi, M. Javaheri, M. Kheirmand, R.A. Mirzai, *Int. J. Hydrogen Energy* 36 (2011) 13325-13334.

37. K.S. Lee, D.M. Kim, *Int. J. Hydrogen Energy* 37 (2012) 6272-6276.

38. Y. Yuan, B. Zhao, Y. Jeon, S. Zhong, S. Zhou, S. Kim, *Bioresour. Technol.* 102 (2011) 5849-5854.

39. Z.S. Yin, T.H. Hu, J.L. Wang, C. Wang, Z.X. Li, J.W. Guo, *Electrochim. Acta* 119 (2014) 144-154.

40. A. Ghosh, S. Basu, A. Verma, *Fuel cell* 13 (2013) 355-363.

41. J. Jin, X. Fu, Q. Liu, J. Zhang, *J. Mater. Chem. A* 1 (2013) 10538-10545.

42. J. Yan, H. Meng, F. Xie, X. Yuan, W. Yu, W. Lin, W. Owgang, D. Yuan, *J. Power Sources* 245 (2014) 772-778.
43. J. Wu, Y. Wang, D. Zhang, B. Hou, *J. Power Sources* 196 (2011) 1141-1144.
44. L. Qu, Y. Liu, J.B. Baek, L. Dai, *ACS Nano* 4 (2010) 1321-1326.
45. E.Y. Kataev, D.M. Itkis, A.V. Fedorov, B.V. Senkovsky, D.Y. Vsachv, N.I. Verbitskiy, A. Gruneis, A. Barinov, D.Y. Tsukanova, A.A. Volykhov, K.V. Mironovich, V.A. Krivchenko, M.G. Rybin, E.D. Obraztsova, C. Laubschat, D.V. Vyalikh, L.V. Yashina, *ACS Nano* 9 (2015) 320-326.
46. Y. Takasu, M. Suzuki, H. Yang, T. Ohashi, W. Sugimoto, *Electrochim. Acta* 55 (2010) 8220-8229.
47. Y. Lin, S. Shrestha, W.E. Mustain, *ACS. Catal.* 2 (2012) 456-463.
48. C.H. Chang, T.S. Yuen, Y. Nagao, H. Yugami, *J. Power Sources* 195 (2010) 5938-5941.
49. J. Wang, F. Meng, T. Xia, Z. Shi, J. Lian, C. Xu, H. Zhao, Z.M. Bassat, J.C. Grenie, *Int. J. Hydrogen Energy* 39 (2014) 18392-18404.
50. C.H. Wang, C.W. Yang, Y.C. Lin, S.T. Chang, *J. Power Sources* 277 (2015) 147-154.
51. B. An, W. Zhou, Y. Guo, R. Ran, Z. Shao, *Int. J. Hydrogen Energy* 35 (2010) 5601-5610.
52. W. Shimizu, K .Okada, Y. Fijta, S.S. Zhao, Y. Murakami, *J. Power Sources* 205 (2012) 24-31.
53. M. Qezaslan, P. Strasser, *J. Power Sources* 196 (2011) 5240-5249.
54. J.C. Cruz, V. Baglio, S. Siracusano, R. Orneals, L.G. Arriaga, V. Antonucci, A.S. Arico, *Int. J. Hydrogen Energy* 37 (2012) 5508-5517.
55. T. Hong, F. Chen, C. Xia, *Electrochem. Commun.*, 51 (2015) 93-97.
56. T. Hong, F. Chen, C. Xia, *J. Power Sources* 278 (2015) 741-750.
57. Y. Cheng, W. Li, X. Feng, J. Liu, W. Xu, C. Yan, *Electrochim. Acta* 111 (2013) 635-641.
58. N. Todoroki, T. Kato, T. Hayashi, S. Takahashi, T. Wadyama, *ACS. Catal.* 5 (2015) 2209-2212.
59. Z. Yan, M. Wang, J. Liu, R. Liu, J. Zhao, *Electrochim. Acta* 141 (2014) 331-339.
60. F.H.B. Lima, J.F.R.D. Castro, A. Ticianelli, *J. Power Sources* 161 (2006) 806-812.
61. H. Gharibi, F. Gomohammadi, M. Kheirmand, *Electrochim. Acta* 89 (2013) 212-221.
62. J.J. Lv, S.S. Li, A.J. Wang, L.P. Mei, J.R. Chen, J.J. Feng, *Electrochim. Acta* 136 (2014) 521-528.
63. A. Maghsodi, M.R.M. Hoseini, M.D. Mobarakeh, M. Kheirmand, L. Samiee, F. Shoghi, M.Kameli, *Appl. Surf. Sci.*257 (2011) 6353-6357.
64. M. Muraoka, H. Tomonaga, M. Nagai, *Fuel cell* 97 (2012) 211-218.
65. B. Andreaus, A.J. McEvoy, G.G. Scherer, *Electrochim. Acta* 47 (2002) 2223-2229.
66. T. Okada, N.I. Wakayama, L. Wang, H. Shingu, J.I. Okano, T. Ozawa, *Electrochim. Acta* 48 (2003) 531-539.
67. E. Antosini, R.R. Passos, E.A. Ticianelli, *Electrochim. Acta* 48 (2002) 263-270.
68. X. Zhou, P. Xu, L. Xu, Z. Bai, Z. Chen, J. Qiao, *J. Power Sources* 260 (2014) 349-356.
69. N. Chattarjee, I.N. Basumallick, *J. Power Sources* 63 (1996) 271-273.
70. R.I. Jafri, N. Sujatha, N. Rajalakshmi, S. Rajalakshmi, S. Ramaprabhu, *Int. J. Hydrogen Energy* 34 (2009) 6371-6376.
71. B.H.R. Suryanto, X. Lu, C. Zhao, *J. Mater. Chem. A* 1 (2013) 12726-12731.
72. K. Tiido, N. Alexeyeva, M. Couillaod, C. Bock, B.R. Macdougal, K. Tammeveski, *Electrochim. Acta* 107 (2013) 509-517.
73. Y. Jiang, Y. Lu, X. Lv, D. Han, Q. Zhang, L. Niu, W. Chen, *ACS catal.*, 3 (2013) 1263-1271.
74. L. Cui, G. Lv, Z. Dou, X. He, *Electrochim. Acta* 106 (2013) 272-278.
75. X. Bo, C. Han, Y. Zheng, L. Guo, *ACS. Appl. Mater. Interfaces* 6 (2014) 3023-3030.
76. R. Loukrakpam, B.N. Wanjala, J. Yin, B. Fang, J. Luo, M. Shao, L. Protsailo, T. Kawamura, Y. Chen, V. Petkov, C.J. Zhang, *ACS. Catal.* 1 (2011) 562-572.
77. Y. Fang, X. Yang, L. Wang, Y. Liu, *J. Power Sources* 267 (2014) 33-38.

78. R. Bresciani, S. Marzorati, A. Lascialfari, B. Sacchi, N. Santo, M. Longhi, *Electrochem. Commun.*, 51 (2015) 27-32.
79. Z. Yan, J. Xie, J. Jing, M. Zhang, W. Wei, S. Yin, *Int. J. Hydrogen Energy* 37 (2012) 15948-15955.
80. Q. Wen, S. Wang, J. Yan, L. Cong, Y. Chen, H. Xi, *Bioelectrochemistry* 95 (2014) 23-28.
81. J. Shi, X. Zhou, P. Xu, J. Qiao, Z. Chen, Y. Liu, *Electrochim. Acta* 145 (2014) 259-269.
82. L. Zhu, D. Susac, M. Teo, K.C. Wong, P.C. Wong, D. Bizzotte, K.A.R. Mitchell, S.A. Campbell, *J. Catal.* 258 (2008) 235-242.
83. R.G.G. Huerta, A.G. Guzman, O.S. Feria, *Int. J. Hydrogen Energy* 35 (2010) 12115-12119.
84. J. Wu, Y. Wang, D. Zhang, B. Hou, *J. Power Sources* 196 (2011) 1141-1144.
85. S. Strbac, I. Srejic, M. Smiljanic, Z. Rokocevic, *J. Electroanal. Chem.*, 704 (2013) 24-31.
86. A.A. Ensafi, M.J. Asl, B. Rezaei, *Electrochim. Acta* 130 (2014) 394-405.
87. Q. Wu, L. Jiang, Q. Tang, J. Liu, S. Wang, G. Sun, *Electrochim. Acta* 91 (2013) 314-322.
88. A. Restovic, E. Rios, S. Barbato, J. Ortiz, J.L. Gautier, *J. Electroanal. Chem.*, 522 (2002) 141-151.
89. S. Baranton, C. Countanceau, C. Roux, F. Hahn, J.M. Leger, *J. Electroanal. Chem.*, 577 (2005) 223-234.
90. J. Liu, X. Jin, W. Song, F. Wang, N. Wang, Y. Song, *Chin. J. Catal.* 35 (2014) 1173-1188.
91. C.P. Gonzalo, O. Kartachova, A.A.J. Torriere, P.C. Howlet, A.M. Glushenkov, D.M. Fabijanic, Y. Chen, S. Poissonnet, M. Forsyth, *Electrochim. Acta* 103 (2013) 151-160.
92. S. Zhao, J. Liu, C. Li, W. Ji, M. Yang, H. Huang, Y. Liu, Z. Kang, *ACS. Appl. Mater. Interfaces* 6 (2014) 22297-22304.
93. N.R. Elezovic, B.M. Babic, V.M. Radmilovic, L.M. Uracar, N.V. Krstajic, *Electrochim. Acta* 56 (2011) 9020-9026.
94. K. Matsubara, K .Waki, *Electrochim. Acta* 55 (2010) 9166-9173.
95. L. Perini, C. Durante, M. Favaro, V. Perazzolo, S. Agnoli, O. Schneider, G. Granozzi, A. Gennaro, *ACS Appl. Mater. Interfaces* 7 (2015) 1170-1179.
96. Y. Liu, S. Shrestha, W.E. Mastain, *ACS catal.*, 2 (2012) 456-463.
97. H. Liu, Y. Cao, F. Wang, Y. Hwang, *ACS Appl. Mater. Interfaces* 6 (2014) 819-825.
98. S.M. Alia, S. Pylypenko, K.C. Neyerlin, D.A. Cullen, S.S. Kocha, B.S. Pivovar, *ACS. Catal.* 4 (2014) 2680-2686.
99. S. Meenakshi, K.G. Nishanth, P. Sridhar, S. Pitchumani, *Electrochim. Acta* 135 (2014) 52-59.
100. D. Villers, S.H. Sun, A.M. Serventi, J.P. Dodelet, *J .Phys. chem B* 110 (2006) 25916-25925.
101. M.S. Saha, Y. Zhang, M. Cai, X Sun, *Int. J. Hydrogen Energy* 37 (2012) 4633-4638.
102. D.C.M. Casillas, H.A. Calderon, V.C. Martinez, O.S. Feria, *Int. J. Hydrogen Energy* 38 (2013) 12674-12680.
103. K. Fugane, T. Mori, D.R. Ou, A. Suzuki, H. Yoshikawa, T. Masuda, K. Vosaki, Y. Yamashita, S. Veda, K. Kobayashi, N. Okazaki, I. Matolinora, V. Matolin, *Electrochim. Acta* 56 (2011) 3874-3883.
104. Y. Yuan, B. Zhao, Y. Jeon, S. Zhong, S. Zhou, S. Kim, *Bioresour. Technol.* 102 (2011) 5849-5854.
105. V.D. Noto, E. Negro, S. Polizzi, K. Vezzu, L. Toniolo, G. Cavinato, *Int. J. Hydrogen Energy* 39 (2014) 2812-2827.
106. C.H. Cheng, J.S. Yuen, Y. Nagao, H. Yugami, *Solid State Ionics* 197 (2011) 49-51.
107. Z. Zhang, K.L. More, K. Sun, Z. Wu, W. Li, *Chem. Mater.* 23 (2011) 1570-1577.
108. M. Liu, L. Guo, S. Kharkuel, H. Wu, H.Y. Ng, S.F. Li, *J. Power Sources* 221 (2013) 381-386.
109. H. Li, H. Ziu, Z. Song, W. Qu, D. Geng, X. Sun, H. Wang, *Int. J. Hydrogen Energy* 36 (2011) 2258-2265.
110. M. Luo, L. Wei, F. Wang, K. Han, H. Zhu, *J. Power Sources* 270 (2014) 34-41.

111. G. Sievers, S. Muller, A. Quade, F. Steffen, S. Jakubith, A. Kruth, V. Brueser, *J. Power Sources* 268 (2014) 255-260.
112. A.N. Golikand, M. Asgari, E. Lohrasabi, *Int. J. Hydrogen Energy* 36 (2011) 13317-13324.
113. X. Zhou, P. Xu, L. Xu, Z. Bai, Z. Chen, J. Qiao, J. Zhang, *J. Power Sources* 260 (2014) 349-356.
114. W.M. Millan, J.J. Thompson, L.G. Arriaga, M.A. Smit, *Int. J. Hydrogen Energy* 34 (2009) 694-702.
115. G. Zhang, Z.G. Shao, W. Lu, F. Xie, X. Qin, B. Yi, *Electrochim. Acta* 103 (2013) 66-76.
116. S. Dsoke, A. Moretti, G. Giuli, R. Marassi, *Int. J. Hydrogen Energy* 36 (2011) 8098-8102.
117. D.H. Jung, S.J. Bae, S.J. Kim, K.S. Nahm, P. Kim, *Int. J. Hydrogen Energy* 36 (2011) 9115-9122.
118. Q. Liu, Y. Zhou, S. Chen, Z. Wang, H. Hou, F. Zhao, *J. Power Sources* 273 (2015) 1189-1193.
119. I. Gatto, A. Stassi, E. Passalacqua, A.S. Arico, *Int. J. Hydrogen Energy* 38 (2013) 675-681.
120. B. Li, X. Zhou, X. Wang, B. Liu, B. Li, *J. Power Sources* 272 (2014) 320-327.
121. X.B. Gong, S.J. You, X.H. Wang, Y. Gan, R.N. Zhang, N.Q. Ren, *J. Power Sources* 225 (2013) 330-337.
122. X.B. Gong, S.J. You, X.H. Wang, J.N. Zhang, Y. Gan, N.Q. Ren, *Biosens. Bioelectron.* 55 (2014) 237-241.
123. B.Y. Sarada, K.S. Dhathathreyan, M.R. Krishna, *Int. J. Hydrogen Energy* 36 (2011) 11886-11894.
124. B. Li, Z. Yan, Q. Xiao, J. Dai, D. Yang, C. Zhang, M. Cai, J. Ma, *J. Power Sources* 270 (2014) 201-207.
125. T. Xu, H. Zhang, Y. Zhang, H. Zhong, H. Jin, Y. Tang, *J. Power Sources* 196 (2011) 5849-5852.
126. N.S. Parimi, Y. Umasankar, P. Alanassov, P. Ramasamy, *ACS. Catal.* 2 (2012) 38-44.
127. T.J. Schmiott, U.A. Paulus, H.A. Gasteiger, R.J. Behm, *J. Electroanal. Chem.* 508 (2001) 41-47.
128. J. Seo, D.H. Anjum, K. Takanabe, J. Kubota, K. Domen, *Electrochim. Acta* 149 (2014) 76-85.
129. P.H. Matter, E. Wang, M. Arias, E.J. Biddinger, U.S. Ozkan, *J. Mol. Catal. A: Chem.* 264 (2007) 73-81.
130. J. Liu, C. Xu, C. Liu, F. Wang, H. Liu, J. Ji, Z. Li, *Electrochim. Acta* 152 (2015) 425-432.
131. H. Gu, H. Chen, L. Gao, Y. Zheng, X. Zhu, L. Guo, *Int. J. Hydrogen Energy* 34 (2009) 2416-2420.
132. F. Liang, W. Zhou, B. Chi, J. Pu, S.P. Jiang, L. Jiang, *Int. J. Hydrogen Energy* 36 (2011) 7670-7676.
133. S. Shanmugam, A. Gedanken, *J. Phys. Chem. C* 113 (2009) 18707-18712.
134. S. Zhao, H. Yin, L. Du, L. He, K. Zhao, L. Chang, G. Yin, H. Zhao, S. Liu, Z. Tang, *ACS Nano* 8 (2014) 12660-12668.
135. G. Liu, G. Zhang, *J. Phys. Chem. C* 112 (2008) 2058-2065.
136. S.S.J. Aravind, S. Ramaprabhu, *ACS Appl. Mater. Interfaces* 4 (2012) 3805-3810.
137. H.Y. Park, D.S. Yang, D. Bhattacharya, M.Y. Song, J.S. Yu, *Int. J. Hydrogen Energy* 39 (2014) 1688-1697.
138. C. Arbizzani, S. Righi, F. Soavi, M. Mastragostino, *Int. J. Hydrogen Energy* 36 (2011) 5038-5046.
139. P.H. Maheswari, R.B. Mathur, *Electrochim. Acta* 54 (2009) 7476-7488.
140. L. Dong, M. Zhou, C. Liu, L. Liu, C. Liu, S. Dong, *Talanta* 81 (2010) 444-448.
141. M. Lu, L. Guo, S. Kharkwal, H. Wu, H.Y. Ng, S.F.Y. Li, *J. Power Sources* 221 (2013) 381-386.
142. Y. Zhang, J. Sun, Y. Hu, S. Li, Q. Xu, *J. Power Sources* 239 (2013) 169-174.